Research paper

Analysis of the relationship between lung cancer drug response level and atom connectivity dynamics based on trimmed Delaunay triangulation

Bin Zou [a,*], Debby D. Wang [b], Lichun Ma [a], Lijiang Chen [a,c], Hong Yan [a]

[a] Department of Electronic Engineering, City University of Hong Kong, Kowloon, Hong Kong
[b] Caritas Institute of Higher Education, 18 Chui Ling Road, Tseung Kwan O, New Territories, Hong Kong
[c] School of Electronic and Information Engineering, Beihang University, China

A B S T R A C T

Epidermal growth factor receptor (EGFR) mutation is a pathogenic factor of non-small cell lung cancer (NSCLC). Tyrosine kinase inhibitors (TKIs), such as gefitinib, are widely used in NSCLC treatment. In this work, we investigated the relationship between the number of EGFR residues connected with gefitinib and the response level for each EGFR mutation type. Three-dimensional trimmed Delaunay triangulation was applied to construct connections between EGFR residues and gefitinib atoms. Through molecular dynamics (MD) simulations, we discovered that when the number of EGFR residues connected with gefitinib increases, the response level of the corresponding EGFR mutation tends to descend.

© 2016 Elsevier B.V. All rights reserved.

1. Introduction

As a worldwide leading cause of cancer deaths, lung cancer accounts for almost 27% of all cancer deaths [1]. Specifically, 85–90% of them are non-small cell lung cancer (NSCLC), with 40–50% diagnosed as in advanced cancer stages [2]. Common treatment strategies such as chemotherapy and radiotherapy have achieved great progresses in recent years, while the overall survival rate of NSCLC patients has not been improved remarkably. For example, platinum-based combined chemotherapy can only result in an effective rate of 17–22% and a median survival time of 7.4–8.1 months [3]. Therefore, much research of NSCLC is needed in order to provide useful information for more effective treatment design.

Epidermal growth factor receptor (EGFR) is an important receptor kinase that exists on cell surface. It can form homo- or heterodimer with a partner once activated by its extracellular ligands [4]. This dimerization can further switch on downstream signaling and cell proliferation. NSCLC development may involve alterations of EGFR-regulated signal transduction pathways, and EGFR mutations can be a common alteration and thus be a pathogenic factor of NSCLC [5]. Tyrosine kinase inhibitors (TKIs), such as gefitinib,

which target the kinase domain of EGFR, are widely applied in the treatments of EGFR-mutated NSCLC patients [6]. A portion of patients normally have a rapid and effective clinical response to gefitinib [5], while others may have a less favorable response. For examples, those with EGFR mutations on exon 19 or 21 respond well to gefitinib, but those with mutations involving exon 20 always suffer resistance to gefitinib [7,8]. T790M is a well-known EGFR mutation that causes gefitinib resistance because T790M can result in an enhanced kinase affinity to adenosine triphosphate (ATP) than most other mutation types [9].

Patients' responses to gefitinib are largely related to their EGFR mutation types. Several computational methods have been developed to characterize EGFR mutations [10–14]. Specially, molecular dynamics (MD) simulations are broadly used to reveal valuable dynamic features of molecules [15] because molecules are in constant motions [16,17]. The significance of molecular motions motivated us to characterize EGFR mutations from a perspective of molecular dynamics. Based on MD simulations, we investigated the behaviors of EGFR mutations by monitoring the EGFR residues in the gefitinib-binding site. These behaviors were revealed by 3D trimmed Delaunay triangulation, which defines connections among adjacent points (atoms) in the 3D space. Also, an EGFR residue is defined to be connected with gefitinib if it is connected to at least one atom of gefitinib. By analyzing the MD position frames of each EGFR mutant, we obtained those residues close to gefitinib for all frames, and further studied response levels based

on these residues. Our explorations can be beneficial to NSCLC studies and treatment design.

2. Methods

2.1. Data collection

The dataset consists of 30 EGFR TK mutation types from 137 EGFR-mutation induced NSCLC patients, which were collected from the Queen Mary Hospital in Hong Kong [18]. For all these patients, gefitinib was used in their treatments and their drug response levels were categorized into four groups (response level = I, II, III and IV, corresponding to complete response, partial response, stable disease and progression disease, respectively). A smaller response level indicates a lower drug resistance level (higher drug response level). The 30 EGFR mutation types include residue substitutions (e.g. L858R, residue substitution of L with R at residue site 858), deletions (e.g. delE746_A750, deletion of residues at sites 746–750), duplications (e.g. dulS768_D770, duplication of residues at sites 768–770) and modifications (e.g. delL747_P753insS, delete residues at sites 747–753 and then insert S). Mutation types L858R (68 cases), delE746_A750 (30 cases) and delL747_P753insS (8 cases) occupy the majority of the patients and others are rare cases. Patients with the same EGFR mutation type may have different drug response levels. To unify the response level in a mutation group, we adopted two principles. The first one is selecting the response level that more than half of the patients in the group have, and the other one is using the average response value. For example, among all the 68 patients in the L858R-mutation group, 50 of them have response levels of II, and thus II is selected to be the response level of this group. Apart from the 30 EGFR mutation types obtained from the Queen Mary Hospital in Hong Kong, L858R_T790M was also added into our dataset. L858R_T790M is a well-acknowledged mutation that can cause strong drug resistance, thus we set the corresponding response level as IV.

Crystal structures of several EGFR mutant-gefitinib complexes, such as L858R (PDB entry 2itz), are available from the Protein Data Bank (PDB) [19]. For other EGFR mutants, computational methods were used to model them. In this paper, mutant-gefitinib complexes structures modeled in [13] were adopted in our studies. All these structures were modeled based on EGFR templates using homology-modeling strategies [20,21].

2.2. Molecular dynamics (MD) simulations

To obtain the motion patterns of EGFR mutant-gefitinib complexes, MD simulations [22] were implemented. MD simulations use numerical methods to simulate physical movements of atoms, molecules and complexes. To be specific, for a system of interacting particles, forces between the particles and their potential energies are calculated using interatomic potentials or molecular mechanics force fields, and trajectories of atoms are obtained by solving Newton's equations of motion.

In order to run a MD simulation, a specific force field should be selected at first. An MD force field includes Hamiltonian (potential energy function) and the related parameters that describe the intra- and intermolecular interactions between the molecules in the system, and the ff99SB force field is selected in our work. Solvating the complex into a solvated environment is the next step. In this type of simulation, the system has periodic boundary conditions, and we used the TIP3P water model, with a 10.0 angstrom buffer around the complex in each direction. Now the system contains the complex, water molecules, and the periodic box information necessary for simulation. We then carry out a series of

equilibration operations to equilibrate the system to a stable state. These operations include an energy minimization on the system for 1000 steps (the first half steps use the steepest descent algorithm and the remaining steps use the conjugate gradient algorithm), a slow heating of the system for 50 ps from 0 k to 300 k, a density equilibration for 50 ps with a weak restraint weight of 2, and a constant-pressure equilibration for 500 ps. For all these operations, SHAKE is performed for bonds involving hydrogen to remove the bond stretching freedom, and Langevin dynamics is used for efficient temperature control. The simulation time (steps) of each equilibration operation is determined by observing the temperature, density, energy (including potential and kinetic energy) and backbone root-mean-square deviation (RMSD) of each system. Once each system achieving a stable state, we perform a production MD with constant temperature at 300 k and constant pressure at 1 atm for 2 ns. During the production MD simulation, we collect the trajectory frames every 2 ps, resulting in a trajectory of 1000 position frames for each system.

2.3. 3D trimmed Delaunay triangulation

For a discrete set of points S in the space of R^3, a triangulation is a subdivision of the convex hull of the points into tetrahedrons whose vertices are the points of S [23]. There exist many triangulation types, and 3D Delaunay triangulation is one of the most frequently used one. In Delaunay triangulation, no point in S is inside the circumscribed sphere of any tetrahedron. Further, if no more than 4 points are co-spherical, then the Delaunay triangulation is unique [24].

3D Delaunay triangulation maximizes the minimum angle of all the angles of the tetrahedrons in the triangulation, and tends to avoid skinny tetrahedrons. For simplicity, we use the 2D Delaunay triangulation as an example for an illustration. Suppose there are four points A, B, C and D in a plane, as shown in Fig. 1, and we have two ways to do the triangulation. One is to construct two triangles ABC and ACD with the common edge AC (see Fig. 1a) and the other one is to construct two triangles ABD and BCD with the common edge BD (see Fig. 1b). Apparently, Fig. 1a does not meet the Delaunay condition while Fig. 1b does.

To determine whether a point is within a triangle's circumcircle, one way is to calculate the determinant in Eq. (1), which is based on the coordinates of involved points. In Fig. 1, points A, B and C are arranged in a counterclockwise order. If D lies inside the circumcircle of ABC, then this determinant should be positive [26].
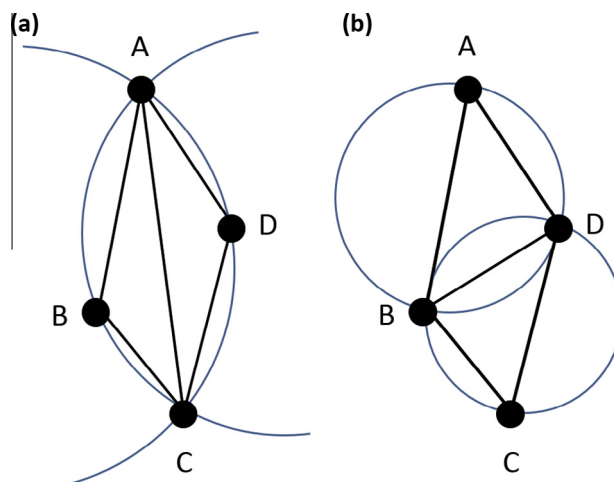
Fig. 1. Two ways to do the triangulation for a four-point set in a 2D plane. (a) A triangulation that does not meet the Delaunay condition. (b) Delaunay triangulation for the point set. This diagram is adopted from [25].

$$\begin{vmatrix} x_A & y_A & x_A^2 + y_A^2 & 1 \\ x_B & y_B & x_B^2 + y_B^2 & 1 \\ x_C & y_C & x_C^2 + y_C^2 & 1 \\ x_D & y_D & x_D^2 + y_D^2 & 1 \end{vmatrix} > 0 \tag{1}$$

If we consider the edges in the triangulation as the connectivity between points, Delaunay triangulation guarantees mostly-close points can be connected. For example, in Fig. 1a where the Delaunay condition is not fulfilled, points A and C are connected, while in a Delaunay triangulation shown in Fig. 1b the relatively closer points B and D are connected.

Delaunay triangulation contains some edges like AB in Fig. 2a where A and B are the outmost points of the point set and their distance is very large. As we need only those edges that can reflect the closeness between points, we should discard these edges from the Delaunay triangulation. To trim long trivial edges, we used a technique applied in alpha shape modeling [27], which is a method based on triangulation to reconstruct the shape formed by a set of points (Fig. 2c). Specifically, if the radius of a circumcircle exceeds a threshold, the longest edge of the corresponding triangle should be discarded. In Fig. 2a, the edge AB should be discarded. The optimal threshold is determined by guaranteeing the point set to form only one connected component. A case in a three-dimensional (3D) space can be similarly extended from the 2D cases, as shown in Fig. 2b. For simplicity, we name the method described above as trimmed Delaunay triangulation.

In this paper, we used 3D trimmed Delaunay triangulation to search those protein residues that are close enough to gefitinib or affect gefitinib directly. Computational Geometry Algorithms Library (CGAL) [28] was applied to model such a triangulation for each system.

2.4. Connectivity between EGFR residues and gefitinib

We monitored the connectivity changes between the EGFR residues and gefitinib in the simulation period. We used 3D trimmed Delaunay triangulation to construct connections between EGFR residues and gefitinib atoms. These connections are dynamic as the structure of the EGFR mutant-gefitinib complex changes in the MD simulations. Tracking such connection changes can reveal the affinities between the EGFR mutants and gefitinib, and thus lead to the derivation of corresponding response levels.

To simplify the problem, we used the alpha carbon atom to represent each EGFR residue. For gefitinib, 30 non-hydrogen atoms were kept. After implementing 3D trimmed Delaunay triangulation, connections were constructed among all residues and the drug atoms. If a residue frequently contacts with gefitinib, its alpha carbon atom would have a higher chance to be connected with at least one gefitinib atom. If more EGFR residues are close enough to the drug molecule, the binding affinity between them will likely be higher. We define an EGFR residue to be connected with gefitinib when its alpha carbon atom is connected to at least one gefitinib atom. For each complex, we then counted the connections between EGFR residues and gefitinib for all simulation frames. By monitoring the connection changes during the whole simulation period, we can obtain convincing results for the mutant-gefitinib affinity studies.

$$B_{p,k,i} = \sum_j A_{p,k,i,j} \tag{2}$$

$$C_{p,k} = \sum_i (B_{p,k,i} > 0) \tag{3}$$

$$D_p = \frac{\sum_{k=1}^N C_{p,k}}{N} \tag{4}$$

The variables in Eqs. (2)–(4) are defined as follows. $A_{p,k,i,j}$ represents the connection between the ith EGFR residue and the jth gefitinib atom in the kth MD frame of the pth EGFR mutation, which takes value 1 when there is a connection and 0 otherwise. $B_{p,k,i}$ is the number of gefitinib atoms that are connected with the ith EGFR residue in the kth MD frame of the pth EGFR mutation. $B_{p,k,i} > 0$ means at least one gefitinib atom is involved in the connection to the ith EGFR residue. $C_{p,k}$ indicates the number of EGFR residues that are connected with gefitinib in the kth MD frame of the pth EGFR mutation. D_p represents the average number of residues connected with gefitinib in the total N frames of the pth EGFR mutation.

3. Results and discussion

We gathered 30 EGFR mutants from 137 NSCLC patients. Their corresponding drug response levels after treatments with gefitinib are shown in Table 1. As described in the method section, we determined the drug response level in each mutation group according to two principles. The first was to select the response level that more than half of the patients in the group had. The other one was to use the average value for this mutation group. In addition, L858R_T790M was also included for a comparison and was assigned a response level of IV.

A series of AMBER [29] MD simulations were implemented for each mutant-gefitinib complex, resulting a trajectory of 1000 frames. Then, we computed connectivity between EGFR residues and gefitinib atoms using 3D trimmed Delaunay Triangulation. To simplify the problem, each EGFR residue was represented by its alpha carbon atom and the hydrogen atoms of gefitinib were excluded. One frame of the L858R-gefitinib complex is shown in Fig. 3. Fig. 3a displays the original ribbon-like complex. Fig. 3b and c present the connectivity in this complex with the vertexes corresponding to protein residues (green) or gefitinib heavy atoms (red), constructed by 3D Delaunay triangulation and 3D trimmed Delaunay triangulation, respectively. We can see that, compared with 3D Delaunay triangulation, 3D trimmed Delaunay triangulation makes only adjacent points connected. In Fig. 3b, the residue in the red circle is connected with gefitinib, but it is actually far from gefitinib and is not connected with gefitinib in Fig. 3c. Gefitinib binding-site residues of EGFR are close to gefitinib and their alpha carbon atoms are most likely to be connected with atoms of gefitinib. We can see that most binding-site alpha carbon atoms are connected with more than one gefitinib atom (Fig. 3d), and thus these residues can influence gefitinib directly.

Afterwards, we counted the number of residues (alpha carbon atoms) connected with gefitinib for each MD frame. Fig. 4 compares the results for L858R/L858R_T790M, delE746_A750/
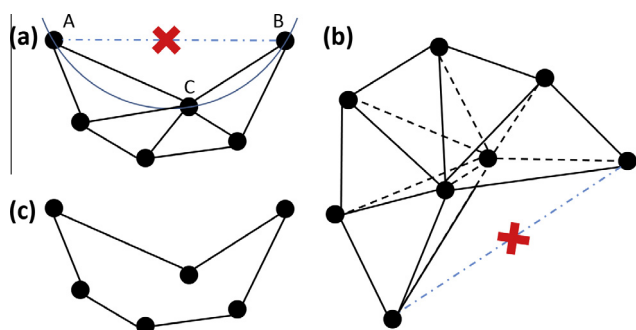

Fig. 2. Trimming long edges in a 2D or 3D Delaunay triangulation. (a) Long edges whose lengths exceed a pre-defined threshold are eliminated, based on alpha shape modeling, in a trimmed Delaunay triangulation. (b) Example of a trimmed Delaunay triangulation in a 3D space. (c) Extracted alpha shape of a set of points in a 2D space.

Table 1
Gefitinib response levels and mutant-gefitinib connectivity measure for 31 EGFR mutants, summarized from 137 patients with EGFR-mutated NSCLC. Specifically, 3 (II) represents that 3 patients have the response level of II to gefitinib. The connectivity measure corresponds to the specific number of mutant residues that are connected with gefitinib.

No.	Mutation name	Response level	Connectivity measure	Comments
1	delE709_T710insD	IV	16.354	1 (IV)
2	delE746_A750	II	21.019	1 (I), 26 (II), 2 (III), 1 (IV)
3	delE746_A750insAP	II	18.519	1 (II)
4	delE746_S752insV	II	18.801	1 (II)
5	delE746_T751insA	III	16.743	1 (III)
6	delE746_T751insI	II	19.679	1 (II)
7	delE746_T751insV	I	21.79	1 (I)
8	delE746_T751insVA	I	20.584	1 (I)
9	delL747_A750insP	III	18.123	1 (II), 1 (IV)
10	delL747_A755insSKG	II	20.829	1 (II)
11	delL747_K754insANKG	IV	15.103	1 (IV)
12	delL747_P753insS	II	17.729	7 (II), 1 (III)
13	delL747_T751	II	20.826	1 (II)
14	delT751_I759insN	II	19.554	1 (II)
15	dulH773	IV	17.871	1 (IV)
16	dulN771_H773	IV	16.034	1 (IV)
17	dulS768_D770	III	18.089	1 (II), 1 (III), 1 (IV)
18	E709A_G719A	IV	17.393	1 (IV)
19	E709K_L858R	II	19.465	1 (II)
20	G719A_L858R	II	19.373	1 (II)
21	G719A_L861Q	II	17.887	1 (II)
22	G719C_S768I	III	16.071	1 (III)
23	G724S_L861Q	IV	19.503	1 (IV)
24	K757R	IV	14.379	1 (IV)
25	L858R	II	22.186	2 (I), 50 (II), 12 (III), 4 (IV)
26	L861Q	II	18.542	2 (II)
27	L861R	IV	18.225	1 (IV)
28	R776H_L858R	II	22.35	1 (II)
29	R831H	III	19.493	1 (III)
30	S768I_V774M	III	18.075	1 (III)
31	L858R_T790M	IV	14.464	

cases, which are consistent with our results. From another perspective, more EGFR residues close enough to the drug molecule may reduce the possibility of drug resistance occurrence, representing a lower value of response level.

Combing all 31 EGFR mutations, we divided them into 4 groups according to their corresponding response levels. Then, we calculated the mean and media number of EGFR residues close to gefitinib for the 4 groups. As Fig. 5 shows, the connectivity curves represent four groups of EGFR mutations, with red, green, blue and magenta ones representing response level groups of I, II, III and IV, respectively. Both the mean (Fig. 5a) and media (Fig. 5c) curves verify the conclusion that more EGFR residues being close to the drug corresponds to a lower value of response level. As a supplementary analysis, Fig. 5c and d shows the mean-connectivity-based and median-connectivity-based moving average curves for the 4 groups, with 9 previous data points used when calculating the moving average of the current data point. These curves present a clearer ranking among the four groups.

We also calculated the average number of residues connected with gefitinib throughout the 1000 frames for each complex (Table 1), and Fig. 6a shows this correlation. The horizontal axis is the mutation index with their drug response level ascending from I to IV. Within each response group, we sorted their average number of residues connected with gefitinib in a descending order. From Fig. 6a we can see that the relation is approximately linear. Although there are overlaps between groups, the trend is clear. It is worth pointing out that, the connectivity measure for L858R or delE746_A750 is much larger than most other mutations, and L858R_T790M corresponds to the smallest connectivity measure. This also supports that L858R and deletion-on-exon-19 mutations respond well to gefitinib while T790M-involved mutations are normally gefitinib-resistant. The average value of each group (shown as stars in Fig. 6a) further verifies our conclusion.

Overall, we derive a conclusion that there is a strong association between the number of residues connected with gefitinib and the EGFR mutation types. Although the trend is clear from Fig. 6a, finding the boundaries among these four groups remains to be our next challenge. Fig. 6b provides a rough partition with a relatively high error rate. If we define response level III and IV representing a drug-resistance case while response levels I and II a drug-response case, we can set a boundary in Fig. 6c where only drug-response and drug-resistance groups are remained. Here the error rate can be reduced significantly. For rare mutations, more patient data are needed to reduce the uncertainty and to further improve our computational model.
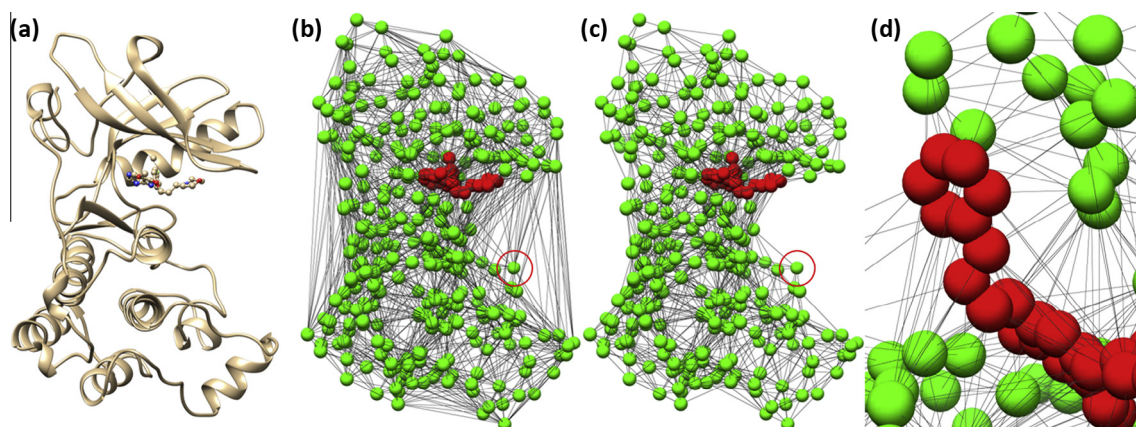
L858R_T790M, delL747_T751/L858R_T790M, and delL747_P753insS/L858R_T790M, respectively. We can see that L858R and deletion-on-exon-19 (delE746_A750, delL747_T751 and delL747_P753insS) mutations have more residues connected with gefitinib than L858R_T790M does, among the 1000 frames. It is widely acknowledged that these EGFR mutations respond well to gefitinib while L858R_T790M causes strong gefitinib-resistance in most

Fig. 3. The connectivity in an L858R-gefitinib complex for a specific frame in the MD simulation period. (a) Original ribbon-like complex. (b) Connectivity in the complex, revealed by 3D Delaunay triangulation, with proteins residues labeled green and gefitinib atoms labeled red. (c) Connectivity in the complex, revealed by 3D trimmed Delaunay triangulation. (d) The binding site connectivity details of the complex. (For interpretation of the references to color in this figure legend, the reader is referred to the web version of this article.)
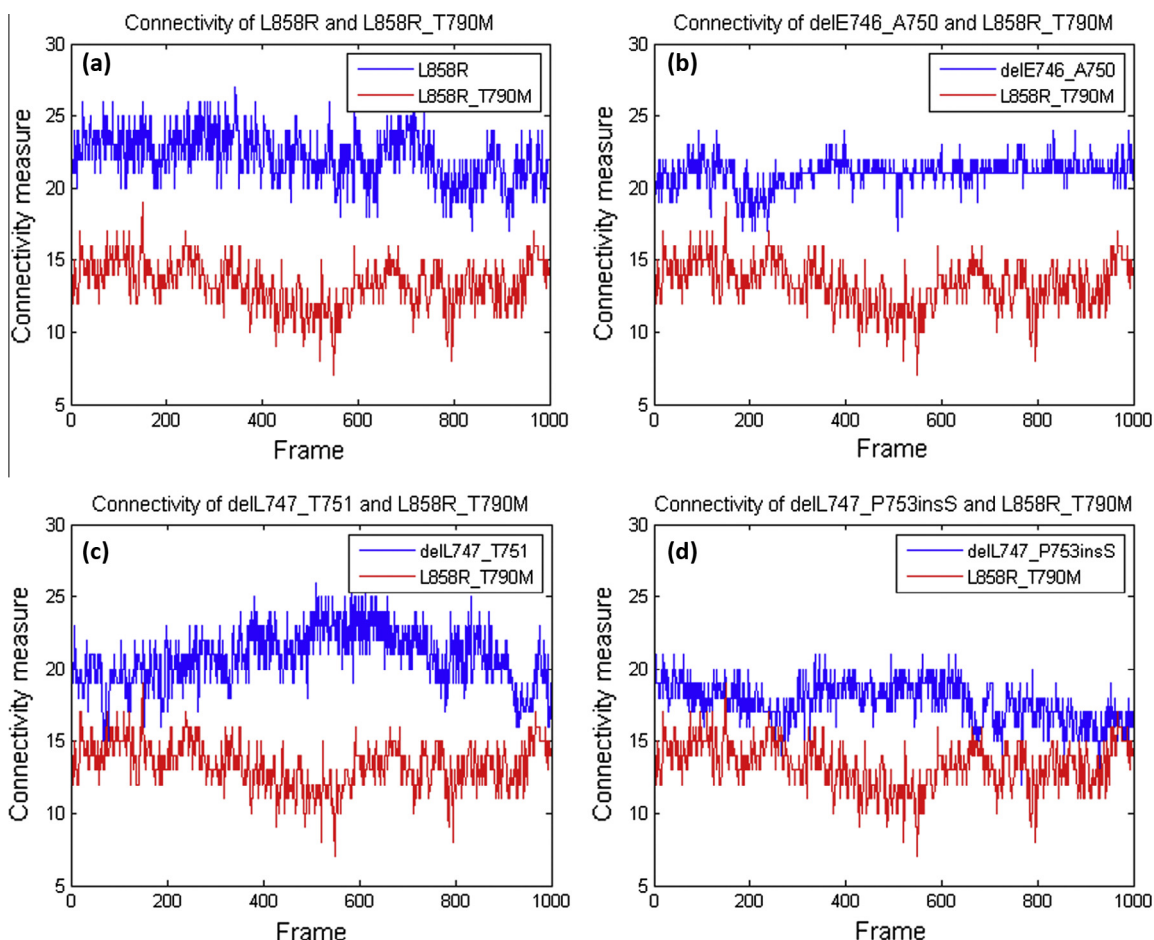
Fig. 4. Comparison of connectivity measures for different EGFR mutation pairs. (a) Comparison between L858R-gefitinib and L858R_T790M-gefitinib complexes. (b) Comparison between delE746_A750-gefitinib and L858R_T790M-gefitinib complexes. (c) Comparison between delL747_T751-gefitinib and L858R_T790M-gefitinib complexes. (d) Comparison between delL747_P753insS-gefitinib and L858R_T790M-gefitinib complexes.
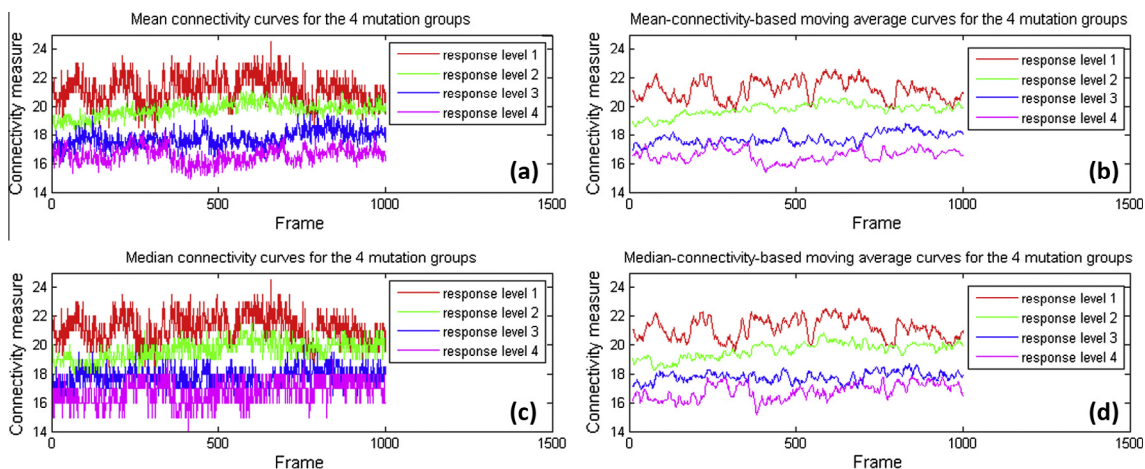

Fig. 5. Connectivity curves corresponding to four groups of EGFR mutations, with red, green, blue and magenta ones representing response level groups of I, II, III and IV, respectively. (a) Mean connectivity curves for the 4 mutation groups. (b) Mean-connectivity-based moving average curves for the 4 mutation groups. (c) Median connectivity curves for the 4 mutation groups. (d) Median-connectivity-based moving average curves for the 4 mutation groups. (For interpretation of the references to color in this figure legend, the reader is referred to the web version of this article.)

4. Conclusion

In this work, we related the number of EGFR residues that are close to gefitinib and the corresponding response level for each EGFR mutation. We studied 137 EGFR-mutated NSCLC patients, corresponding to 30 EGFR mutations, and an additional EGFR mutation L858R_T790M. MD simulations were implemented to simulate the motions of EGFR mutant-gefitinib complexes, and a trajectory of 1000 position frames was obtained for each complex. For each position frame, 3D trimmed Delaunay triangulation was
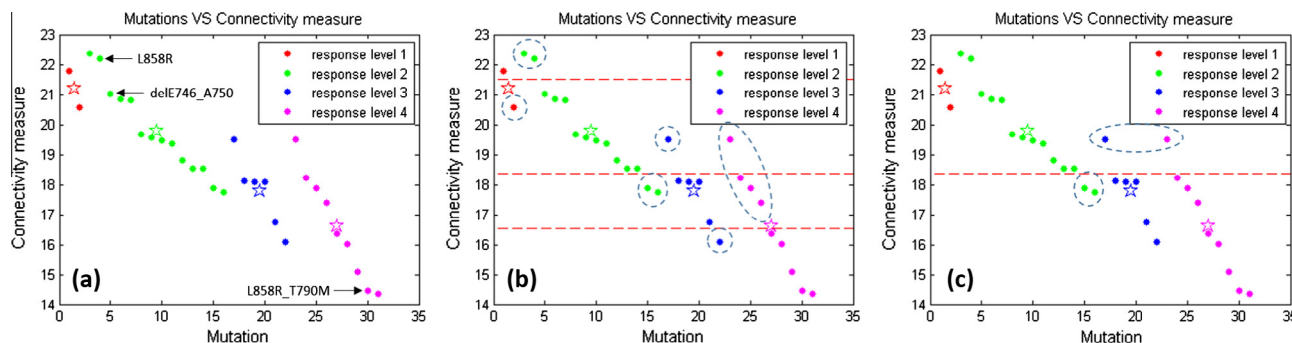
Fig. 6. Correlation analysis of EGFR mutations and the corresponding average connectivity measure. (a) A rough linear relation for the 4 response-level groups, within each of which the connectivity measures are sorted in a descending order for the corresponding mutations. The stars represent the average values of the four groups. (b) Connectivity boundaries for the 4 response-level groups, with an error rate of 11/31. (c) A two-section boundary that divides EGFR mutations into drug-response group and drug-resistance group, with a reduced error rate of 4/31.

applied to construct connections between EGFR residues and gefitinib atoms. Those EGFR residues that connected with any atom of gefitinib were defined to be close to gefitinib. We calculated the average number of EGFR residues close to gefitinib for the 1000 position frames and derived a conclusion that as the number of EGFR residues close to gefitinib increases, the response level of the corresponding EGFR mutation tends to descend, which means patients with the corresponding EGFR mutation are more likely to response well to gefitinib. The findings here can lead us a better understanding of dynamic features of EGFR mutant-gefitinib complexes, and establish a useful link between these features and patients' responses to gefitinib. Our studies provide a useful reference for personalized NSCLC treatment plan.

Acknowledgement

References

[1] R.L. Siegel, K.D. Miller, A. Jemal, Cancer statistics, 2015, CA: Cancer J. Clin. 65 (2015) 5–29.
[2] N.J. Petrelli, E.P. Winer, J. Brahmer, S. Dubey, S. Smith, C. Thomas, et al., Clinical Cancer Advances 2009: major research advances in cancer treatment, prevention, and screening – a report from the American Society of Clinical Oncology, J. Clin. Oncol. 27 (2009) 6052–6069.
[3] F. Ciardiello, R. Caputo, R. Bianco, V. Damiano, G. Pomatico, S. De Placido, et al., Antitumor effect and potentiation of cytotoxic drugs activity in human cancer cells by ZD-1839 (Iressa), an epidermal growth factor receptor-selective tyrosine kinase inhibitor, Clin. Cancer Res. 6 (2000) 2053–2063.
[4] D.D. Wang, L. Ma, M.P. Wong, V.H. Lee, H. Yan, Contribution of EGFR and ErbB-3 Heterodimerization to the EGFR Mutation-Induced Gefitinib-and Erlotinib-Resistance in Non-Small-Cell Lung Carcinoma Treatments, PLoS ONE 10 (2015) e0128360.
[5] T.J. Lynch, D.W. Bell, R. Sordella, S. Gurubhagavatula, R.A. Okimoto, B.W. Brannigan, et al., Activating mutations in the epidermal growth factor receptor underlying responsiveness of non-small-cell lung cancer to gefitinib, New England J. Med. 350 (2004) 2129–2139.
[6] R.S. Herbst, A.-M. Maddox, M.L. Rothenberg, E.J. Small, E.H. Rubin, J. Baselga, et al., Selective oral epidermal growth factor receptor tyrosine kinase inhibitor ZD1839 is generally well-tolerated and has activity in non-small-cell lung cancer and other solid tumors: results of a phase I trial, J. Clin. Oncol. 20 (2002) 3815–3825.
[7] J. Bar, A. Onn, Overcoming molecular mechanisms of resistance to first-generation epidermal growth factor receptor tyrosine kinase inhibitors, Clin. Lung Cancer 13 (2012) 267–279.
[8] H. Greulich, T.-H. Chen, W. Feng, P.A. Jänne, J.V. Alvarez, M. Zappaterra, et al., Oncogenic transformation by inhibitor-sensitive and -resistant EGFR mutants, PLoS Med 2 (2005) e313.

[9] C.-H. Yun, K.E. Mengwasser, A.V. Toms, M.S. Woo, H. Greulich, K.-K. Wong, et al., The T790M mutation in EGFR kinase causes drug resistance by increasing the affinity for ATP, Proc. Natl. Acad. Sci. 105 (2008) 2070–2075.
[10] B. Duan, B. Zou, D.D. Wang, H. Yan, L. Han, Computational evaluation of EGFR dynamic characteristics in mutation-induced drug resistance prediction, in: 2015 IEEE International Conference on Systems, Man, and Cybernetics (SMC), 2015, pp. 2299–2304.
[11] L. Ma, D.D. Wang, Y. Huang, M.P. Wong, V.H. Lee, H. Yan, Decoding the EGFR mutation-induced drug resistance in lung cancer treatment by local surface geometric properties, Comput. Biol. Med. 63 (2015) 293–300.
[12] L. Ma, D.D. Wang, Y. Huang, H. Yan, M.P. Wong, V.H. Lee, EGFR Mutant Structural Database: computationally predicted 3D structures and the corresponding binding free energies with gefitinib and erlotinib, BMC Bioinformatics 16 (2015) 1.
[13] D.D. Wang, W. Zhou, H. Yan, M. Wong, V. Lee, Personalized prediction of EGFR mutation-induced drug resistance in lung cancer, Sci. Rep. 3 (2013).
[14] W. Zhou, D.D. Wang, H. Yan, M. Wong, V. Lee, Prediction of anti-EGFR drug resistance base on binding free energy and hydrogen bond analysis, Proceeding of IEEE Symposium on Computational Intelligence in Bioinformatics and Computational Biology (CIBCB), 2013.
[15] A.L. Jonsson, K.A. Scott, V. Daggett, Dynameomics: a consensus view of the protein unfolding/folding transition state ensemble across a diverse set of protein folds, Biophys. J . 97 (2009) 2958–2966.
[16] D.D. Wang, H. Yan, The relationship between periodic dinucleotides and the nucleosomal DNA deformation revealed by normal mode analysis, Phys. Biol. 8 (2011) 066004.
[17] D.D. Wang, H. Yan, Transcriptional protein-protein cooperativity in POU/HMG/DNA complexes revealed by normal mode analysis, Comput. Math. Methods Med. 2013 (2013).
[18] V.H. Lee, V.P. Tin, T.-s. Choy, K.-o. Lam, C.-w. Choi, L.-p. Chung, et al., Association of Exon 19 and 21 EGFR Mutation Patterns with Treatment Outcome after First-Line Tyrosine Kinase Inhibitor in Metastatic Non-Small-Cell Lung Cancer, J. Thoracic Oncol. 8 (2013) 1148–1155.
[19] H.M. Berman, J. Westbrook, Z. Feng, G. Gilliland, T. Bhat, H. Weissig, et al., The protein data bank, Nucl. Acids Res. 28 (2000) 235–242.
[20] Z. Xiang, B. Honig, Extending the accuracy limits of prediction for side-chain conformations, J. Mol. Biol. 311 (2001) 421–430.
[21] Z. Xiang, C.S. Soto, B. Honig, Evaluating conformational free energies: the colony energy and its application to the problem of loop prediction, Proc. Natl. Acad. Sci. 99 (2002) 7432–7437.
[22] J. Haile, Molecular Dynamics Simulation, vol. 18, Wiley, New York, 1992.
[23] N. Amenta, D. Attali, O. Devillers, Complexity of Delaunay triangulation for points on lower-dimensional polyhedra, RR-5986, INRIA, Research Report2006.
[24] D.-T. Lee, B.J. Schachter, Two algorithms for constructing a Delaunay triangulation, Int. J. Comput. Inform. Sci. 9 (1980) 219–242.
[25] L.E. Kavraki, Geometric Methods in Structural Computational Biology. March 17, 2009. <http://cnx.org/contents/f5c31f8e-7807-4c76-95f8-657d9251fdfb@6.3>.
[26] L. Guibas, J. Stolfi, Primitives for the manipulation of general subdivisions and the computation of Voronoi, ACM Trans. Graph. (TOG) 4 (1985) 74–123.
[27] H. Edelsbrunner, E.P. Mücke, Three-dimensional alpha shapes, ACM Trans. Graph. (TOG) 13 (1994) 43–72.
[28] J.-D. Boissonnat, O. Devillers, M. Teillaud, M. Yvinec, Triangulations in CGAL, in: Proceedings of the Sixteenth Annual Symposium on Computational Geometry, Hong Kong, China, 2000, pp. 11–18.
[29] D. Case, T. Darden, T.E. Cheatham III, C. Simmerling, J. Wang, R. Duke, et al., AMBER 12, vol. 1, University of California, San Francisco, 2012.